

Factors affecting the use of impedance spectroscopy in the characterization of the freezing stage of the lyophilization process: The impact of liquid fill height in relation to electrode geometry

Geoff Smith\*, Muhammad Sohail Arshad, Eugene Polygalov, Irina Ermolina

AAPS PharmSciTech

\*Corresponding Author

Journal	AAPS PharmSciTech
Date Submitted	July 26, 2013
Date revised	Oct 29, 2013
Date Accepted	Nov 15, 2013

Email: [gsmith02@dmu.ac.uk](mailto:gsmith02@dmu.ac.uk)

Phone: +44 115 250 6298

Postal Address: Leicester School of Pharmacy, De Montfort University, Leicester, LE1 9BH, UK

## Abstract

The aim of this study was to investigate the application of impedance spectroscopy using fixed electrode geometries on a standard glass vial in the characterization of the freezing process of solutions at different fill liquid volumes. Impedance spectra (between  $10^{-10}$  to  $10^6$  Hz) were recorded every 3 min, during the freezing cycle on a solution of 3% w/v sucrose contained within 10 mL glass vials having an electrode system (two thin copper foils: w:18 mm; h: 5 mm) affixed to the external surface of the vial. A fill factor ( $\phi$ ) was defined in terms of the relative height of the solution volume to the height of the electrodes from the base of the vial. Solution volumes of 1.5 to 5 ml (corresponding to  $\phi = 0.5$ -1.6) were investigated to establish the applicability of having a fixed electrode geometry for a range of solution volumes. A linear relationship between the time duration of the ice formation/solidification phase and the fill factor suggests that fixed electrode geometries may be used to investigate a range of fill volumes. The benefit of this approach is that it does not invade the solution and hence records the freezing process without providing additional nucleation sites and in a manner which is representative of the entire fill volume.

**KeyWords:** Impedance spectroscopy; freezing; fill height; sucrose

## 1 Introduction

2 Freeze-drying (lyophilisation) is widely practiced in the manufacture of injectable pharmaceuticals to preserve the  
3 stability of the therapeutic agent and to facilitate storage at room temperature (1). The process comprises three  
4 discrete stages: freezing, primary drying and secondary drying. Of these stages, it is the freezing stage that defines  
5 the ice matrix structure and hence the porosity of the dry layer through which water vapour migrates during the  
6 subsequent primary drying stage (2-5). The ice morphologies that were developed on freezing are impacted by  
7 various factors, including the presence of foreign objects and the topography of the container walls, which provide  
8 nucleating sites for subsequent ice growth, the degree of super-cooling and the fill height of liquid in the vial (5-8).

9 The characteristics of the freezing process have been evaluated indirectly from retrospective analysis of the primary  
10 drying stage (i.e. dry layer resistance using process analytical tools) or from measurements of the pore structure of a  
11 freeze dried cake at the end of the cycle (by microCT tomography) (5, 9). Those studies which attempt to examine  
12 the freezing process by direct means are invariably undertaken by off-line techniques, viz. freeze-drying microscopy  
13 and differential scanning calorimetry (10). However the results are of limited relevance due to the fact that the  
14 cooling rate and the degree of super-cooling differ from the real vial conditions, principally due to the differences in  
15 sample geometry and differences in cleanliness of a manufacturing environment and a lab environment.

16 The conventional in-line method for characterizing the freezing step is to use a thermocouple inserted into the  
17 product to monitor changes in temperature associated with the exothermic crystallization of ice (11, 12). However,  
18 by virtue of the fact that the probe resides within the liquid, then the physical presence of the probe necessarily  
19 perturbs the processes of ice nucleation and solidification, through the introduction of nucleation sites and thermal  
20 inputs respectively. This may result in ice structures which are **different from those** that would otherwise develop  
21 within the regular (non-thermocouple containing) vials (13). Alternatively the thermocouple probe is attached to the  
22 external surface (base) of the vial to avoid product invasion. Nevertheless, being a single point measurement tool,  
23 the data derived from a thermocouple measurement may not provide a true representation of the entire fill volume  
24 (6).

25 Other techniques, including near infra-red (NIR) spectroscopy, Raman spectroscopy and optical tomography (14-16)  
26 are also used to study the freezing profile. Challenges associated with these technologies include i) the placement of  
27 a thermocouple probe with in the vial will inevitably impact/perturb the processes of ice formation ii) bulky  
28 technologies, such as NIR and Raman probes, which require close placement to the vial in question, do not permit  
29 the usual hexagonal arrangement of vials on the freeze drier shelf and therefore provide limited access to those vial  
30 in the centre of the cluster.

31 Impedance spectroscopy (IS) concerns the response of a material to an applied electric field. The response may  
32 range from the delocalised charge phenomenon of ionic conduction, through localised space charge polarization  
33 (e.g. interfacial polarization of the boundaries between two phases) to true dielectric phenomenon such as dipole re-  
34 orientation. The majority of applications for IS are for the analysis of materials in which ionic conduction  
35 predominates (e.g. solid and liquid electrolytes), for example in the study of fuel cells, rechargeable batteries, and  
36 corrosion. There are fewer, but equally important, applications for impedance spectroscopy in the study of dielectric  
37 materials (i.e. solid or liquid non-conductors whose electrical characteristics involve dipolar rotation, e.g. glasses and  
38 polymers) and for those materials whose mechanism of conduction is predominantly electronic (e.g. single-crystal or  
39 amorphous semiconductors)(17). Invariably the term dielectric spectroscopy is adopted in preference to IS for the  
40 latter types of materials, as the main focus for investigation is the thermally damped relaxation of molecular dipoles.  
41 However, many materials do not fall into one category or another, and so IS often finds uses in more complex  
42 situations, such as a partly conducting dielectric material with some ionic conductivity. Pharmaceutical materials are  
43 a good example of this latter type of material, with even the driest of materials (e.g. powders and granules)  
44 exhibiting protonic conduction processes which percolate through the hydration surface of a powder (18, 19), whilst  
45 displaying pronounced dielectric relaxation phenomena associated with dipole reorientation (20). Despite numerous  
46 scientific studies on a wide range of material types, the application for IS for industrial process control is much less  
47 prevalent, with the most well-known being the monitoring of the fermentation process in the brewing industry (21,  
48 22).

49 The recent exploration of the use of IS for the characterization of the lyophilisation process (23) has shown  
50 that the cooling rate, the freezing process and the end point of primary drying may be monitored by the application

51 of electrodes external to the vial. The reason why this approach has worked in practice is that the electrical  
52 impedance of the object is a function of both the dielectric and conductive properties of the assembly which are, in  
53 turn, defined by the composition and physical state of the material contained within the vial, the temperature of the  
54 assembly, and the geometry of the vial and electrode system. The first article demonstrated the application of  
55 impedance spectroscopy in defining the end point of primary drying, which was determined from the inflection in  
56 the derivative profile of the imaginary capacitance (dielectric loss) at 1 kHz. The technology described in that  
57 publication, comprised a pair of stimulating and sensing electrodes affixed close to the base of a glass vial (10 ml).  
58 Each electrode has dimensions 18x5 mm, and is surrounded by a guard electrode to prevent leakage of the electrical  
59 field. The height of each electrode measures 1 cm from the base of the vial (which cover a 3 ml volume in the vial)  
60 (24).

61 An understanding of the position and dimensions of the electrodes in relation to the volume (fill height)  
62 occupied by the liquid, for a range of vial sizes, is necessary to the general application of this approach in freeze-  
63 drying process development. The obvious first question is how the liquid fill height will impact the impedance  
64 spectra recorded by the measurement instrument and the second question is how universal this type of  
65 measurement might be for a range of vial sizes.

66 The first question will be addressed in the main body of this article through an experimental study on  
67 conventional 10 mL vial (Schott) with a fill volume ranging from 1.5 to 5 mL, corresponding to a fill height of 0.5 to  
68 1.7 cm. The height of the electrodes was fixed at 1 cm from the bottom of the vial, and electrical impedance profiles  
69 were recorded for a fill volume of 3 ml which provides a fill depth of 1 cm and fill factor ( $\phi$ ) of 1 (ratio of sample  
70 height to the height of the top of the guard electrode). In practice, the fill depth may increase up to 2 cm (equivalent  
71 to  $2\phi$  (6ml)). The measurements of electrical responses at these fill heights will define the potential of the  
72 impedance spectroscopy in monitoring of the freeze-drying process at variable fill volumes. Fill heights > 2 cm should  
73 be avoided where possible as it may result in high intra-vial variability and poor cake appearance due to altered heat  
74 flow during freezing and primary drying (6).

75 The second question, in relation to the opportunity to measure the freezing characteristics of solutions  
76 within other sizes of vials, is examined theoretically through calculations of the shift in the relaxation frequency of

77 the interfacial polarization process with changes to the diameter of the vial. The methodology and results of these  
78 calculations have been given in Appendix 1.

79 The final aspect to investigate, when considering different vial geometries and the associated differences in  
80 the design/geometry of the electrodes, is the impact of the additional electrode mass on the thermal characteristics  
81 of the vial; as there is potential for the additional mass to impact heat transfer to the vial and the rate of freezing  
82 and/or drying experienced by the modified vials. The starting point for this analysis is to define a theoretical limit of  
83 the thermal mass contributed by the electrodes as ~1% of the vial weight. For the 10 ml tubing vials, used in the  
84 through-vial impedance measurements, the electrode mass was measured and found to be ~ 1.4% of the vial weight.  
85 For other sizes of vial, it is also necessary to estimate whether the electrode mass is within the theoretical limit of  
86 ~1%. To make this assessment, some calculations were made to determine the mass of the electrode system for  
87 different sized glass vials, viz. 2ml, 4ml, 6ml and 8ml glass vials. The same calculation was undertaken for the 10 ml  
88 vial in order to demonstrate the validity of these thermal mass calculations. The methodology and results from these  
89 calculations are given in Appendix 2.

## 91 **Materials**

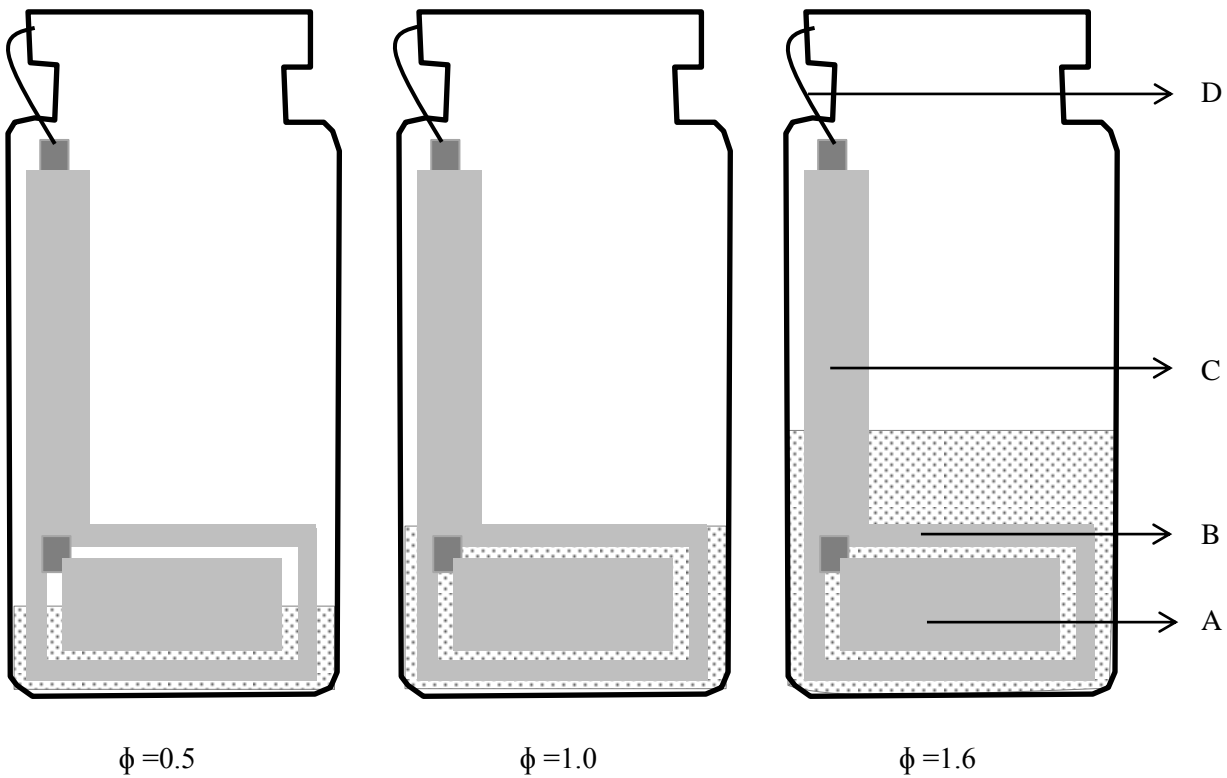
92 Sucrose, purchased from Sigma Aldrich UK, was used as supplied.

## 93 **Methods**

94 A 30 mg/ml sucrose solution was prepared in single distilled water obtained from all glass apparatus. Aliquots of the  
95 sucrose solution were transferred to impedance measurement vials (N=5) via a 0.2 micron micro filter (Minisart,  
96 Germany). The impedance measurement vial is a clear glass 10 ml freeze-drying tubing vial (Schott) with two copper  
97 foil electrodes (18x5 mm) attached at the external bottom curvature and connected at the vial neck to a pair of  
98 miniature coaxial cables via longitudinal copper foil strips. Also a thin guard electrode was applied around each of  
99 the stimulating and sensing electrodes to prevent electrical leakage during the impedance measurement (Figure 1).

100 The measurement vials were connected to a high precision impedance analyser located outside of the freeze drier  
101 (HETO FD08, Denmark) via a junction box and a hermetically sealed pass-through. The impedance spectrum was  
102 recorded by scanning the frequencies in the range  $10^1$ - $10^6$  Hz. The acquisition time for each spectrum was 27 s and  
103 an interval between all five measurements of 3 min. The product temperature was recorded by means of type K  
104 thermocouple placed in the glass vials, arranged in a line on the shelf, using temperature data logger OctTemp 2000  
105 (Madgetech USA).

106 The fill volume was successively increased from 1.5 to 5 ml. Each freezing experiment was repeated to provide ten  
107 measurements at each fill volume. The corresponding solution fill height ranged from  $\sim$  4.6 mm (1.5ml) which sits  
108 below the electrode foil height of 10.5mm, to 17.5 mm (5.0 ml), which sits above the top of the electrodes. These  
109 product fill heights correspond to a fill factor ( $\Phi$ ) increasing from 0.5 to 1.6. (Figure 1)



111 **Figure 1** Electrodes attached to the outside of a freeze-drying vial. A is the active electrode, B is the guard electrode,  
 112 C is the connector strip from the electrode to the neck of the vial, D is the miniature co-axial wire connecting the  
 113 electrode to the measuring system (where the outer braiding of the coaxial cable attaches to the guard electrode  
 114 and the inner conductor attaches either to the stimulating or current sensing electrode ( $\phi$  is the ratio of liquid fill  
 115 height to the height of the top of the guard electrode )

116 The freezing cycle comprised the following steps: (1) Temperature ramp to 25 °C, over 10 min; (2) Hold temperature  
 117 at 25 °C for 20 min; (3) Temperature ramp to -30 °C, over 60 minutes; (4) Hold temperature at -30 °C for 120 min.

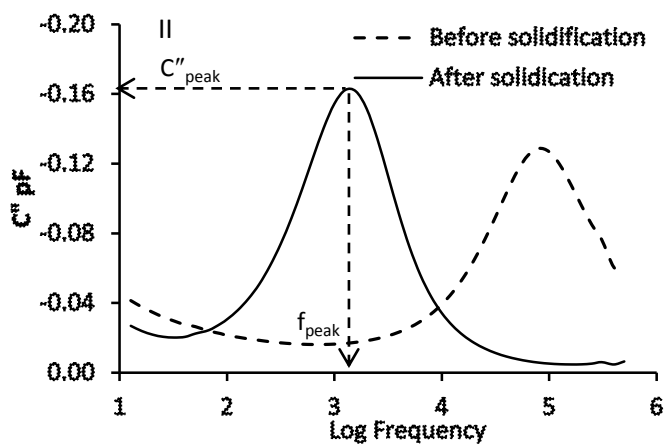
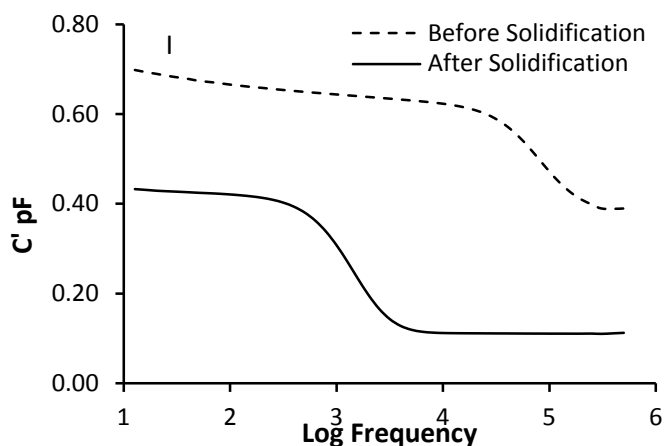


119 **Results and Discussion**

120 The basic characteristics of the freezing process are described first for a fill factor of  $\phi=1$  while the impact of fill  
121 height is evaluated in the next section.

122 **Freezing Characteristics at fill factor,  $\phi=1$**

123 At a fill factor of  $\phi=1$  the capacitance spectrum of the material under test (i.e. glass vial and the 30 mg/ml sucrose  
124 solution) displayed a step-like decrease in the **real part of the electrical** capacitance as the frequency is increased  
125 through the critical frequency which corresponds to the relaxation time constant for the sample ( $f = 1/2\pi\tau$ ) (Fig. 2 I).  
126 There is a corresponding peak in the associated imaginary capacitance (dielectric loss) spectrum as the material  
127 under test starts to conduct electricity through the phase lag between the response of the sample and the applied  
128 electric field (Fig. 2 II). **The real part of capacitance refers to that component of the capacitance which is in phase**  
129 **with the reactive current and the imaginary capacitance refers to that component of the capacitance that is out of**  
130 **phase with the reactive current.** The manifestation of the step in the real part of capacitance and the peak in the  
131 imaginary **part of** capacitance is known as a pseudo-relaxation process, as it has the appearance of a real relaxation  
132 process within a material (i.e. one that has a frequency dependence to its dielectric properties owing to some  
133 molecular relaxation or some form of interfacial charging within the material). In reality the dielectric properties of  
134 the material within the vial may be static i.e. invariant with frequency, and **the pseudo-relaxation process is simply**  
135 **due to** the accumulation of charge at the glass surface as ions migrate through the liquid (or solid) contained within  
136 the glass vial. A more appropriate description of the pseudo-relaxation process is therefore 'an interfacial  
137 polarization' process.



138

139

140

141

**Figure 2** Capacitance plots during the freezing of a sucrose solution (30 mg/ml) (I) left shows the frequency dependence of the real part of capacitance ( $C'$ ) and (II) right shows the frequency dependence of the imaginary part of capacitance ( $C''$ ) The dotted line represents liquid state and the solid line denotes frozen state.

142

143

144

145

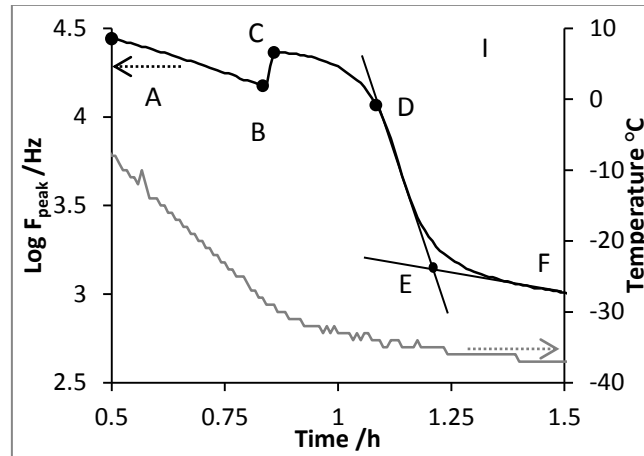
146

147

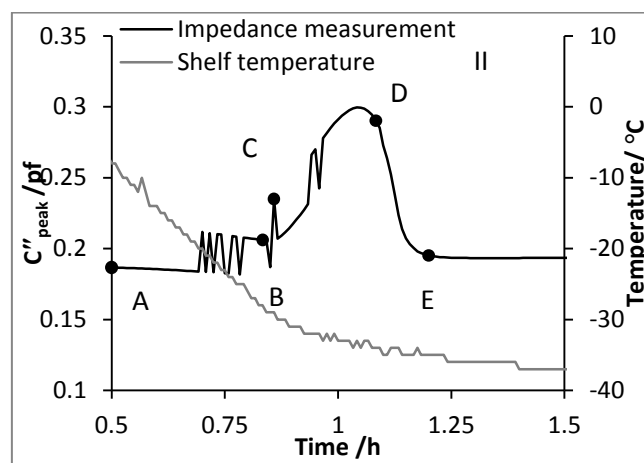
148

The features of the pseudo-relaxation process as a function of time were characterized in terms of the amplitude ( $C''_{\text{peak}}$ ) and frequency position ( $f_{\text{peak}}$ ) of the peak in the imaginary capacitance spectrum (Fig. 2II). The time profile of  $\log f_{\text{peak}}$  (Fig 3 I) is remarkably similar to that recorded by the thermocouple (Fig 3 II) and identifies various phases in the freezing cycle: the pre-cooling phase (A to B), the onset of ice formation (point B), the solidification phase of the product (i.e. the ice growth phase) (B to D) and the subsequent equilibration of the product temperature with the shelf temperature (D to E). In contrast the time profile of  $C''_{\text{peak}}$  (Fig 3 III) is quite different and somewhat scattered, up to the point of complete solidification (point D).

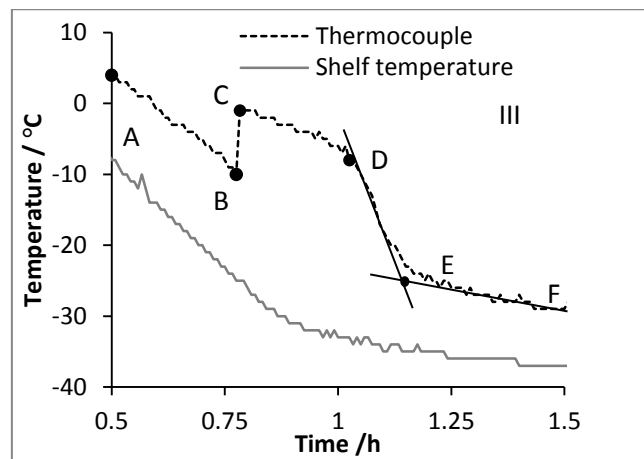
149



150



151



152 **Figure 3.** Time profile of (I) the peak frequency ( $f_{\text{peak}}$ ), (II) the peak amplitude ( $C''_{\text{peak}}$ ) and (III) product temperature  
 153 of sucrose 30mg/ml during freezing. **Plots I and III clearly** identify critical steps relating to product freezing; A to B is  
 154 product cooling (pre-ice formation), B is the onset of ice formation, C describes the maximum increase in product  
 155 temperature following exothermic heat dissipation during ice formation. From these transitions one can define B-D  
 156 as the ice solidification phase, D-E as the equilibration phase, E-F is product cooling II (**post ice formation**).  $C''_{\text{peak}}$

157 appears noisy during the freezing but delineates precisely the end point of the equilibration phase (point E). **Note**  
158 **that time zero is taken from the end of the equilibration phase after the vial and contents have been maintained at**  
159 **25 °C for 10 min.**

160 Further explanation of each phase is given **below**:

161 **Cooling Phase (A to B)** The magnitude of  $\log f_{\text{peak}}$  decreases linearly with the time because of the temperature  
162 dependent decrease in the electrical resistance of the sucrose solution. This behaviour continues until the ice  
163 nucleation point is reached (point B).

164 **Ice Nucleation (point B)** The onset of freezing or **ice nucleation** is identified by an abrupt increase in the magnitude  
165 of  $f_{\text{peak}}$  which results from the elevation in temperature, following the release of the heat of ice crystallization (an  
166 exothermic process). The time corresponding **to this transition** was recorded as the nucleation time.

167 **Solidification Phase (B-D)** As the ice **onset** phase (nucleation) progresses to the growth of ice crystals, it is the rate of  
168 ice formation that defines the rate of energy release into the product and hence the rate of the temperature rise.  
169 However, in parallel with the increase in temperature from ice formation, there is also an increase in the rate of heat  
170 dissipation through the walls of the vial. At some point, the rate of ice formation slows down, such that the rate of  
171 heat dissipation then exceeds the rate of heat release and the temperature then starts to decrease. This defines the  
172 point C. Thereafter, the heat dissipation rate dominates the energy balance in the system and the temperature  
173 begins to return to equilibrium with the shelf (point E). However, before equilibrium is reached there comes a point  
174 when no more ice forms in the system and energy dissipation alone defines the energy balance in the system. The  
175 time period from point B to point D is therefore defined as the solidification time, during which the ice crystallization  
176 process is complete, whereas the time period from **D to E** defines the **equilibration phase**.

177 **Cooling Phase II (E-F)** Following the equilibration phase, the contents of the vial continue to cool at rate defined by  
178 the cooling rate of the shelf; Though the thermal exchange between the vial contents and the surroundings means  
179 that the temperature within the vial stabilize 1-2 °C above the shelf **temperature**.

180 The end of the equilibration phase (E) was estimated from the point where the tangent of the line through the data  
181 from the solidification phase intersects with the tangent of the line through the data from cooling phase II (post ice  
182 formation). The **freezing time** is then defined as the time difference from point B to E. The time duration of each  
183 phase was also estimated from the product temperature profile recorded by the thermocouple (Fig. 3II).

#### 184 **Freezing characteristics of sucrose 30 mg/ml at different fill factors ( $\phi=0.5$ to 1.6)**

185 The features of pseudo-relaxation process were also assessed at two other fill factors ( $\phi= 0.5$  and  $\phi= 1.6$ ). Both log  
186  $f_{\text{peak}}$  and temperature profiles show that by increasing the fill volume (so that the fill factor changes from 0.5 to 1.6)  
187 results in the prolongation of the freezing process (fig 4). The analysis of these profiles, along the lines-described  
188 earlier, provides a range of estimates for the ice nucleation time, the freezing time, the solidification time and the  
189 equilibration time. In each plot, the cumulative standard deviation takes in account the variability in freezing times  
190 associated with the position of vials on the shelf in relation to the walls of the drier, and the small differences in vial  
191 geometry.

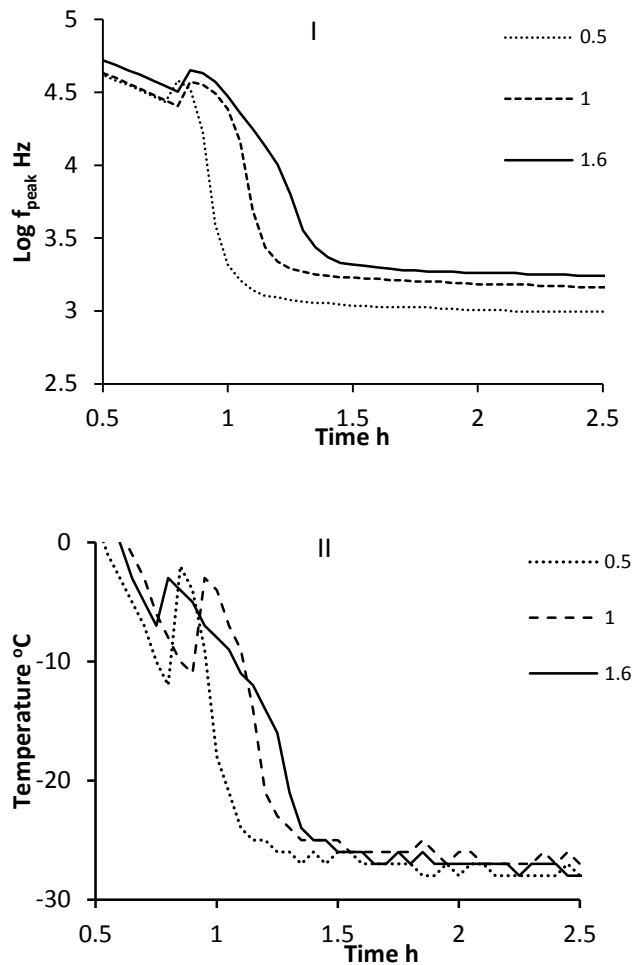
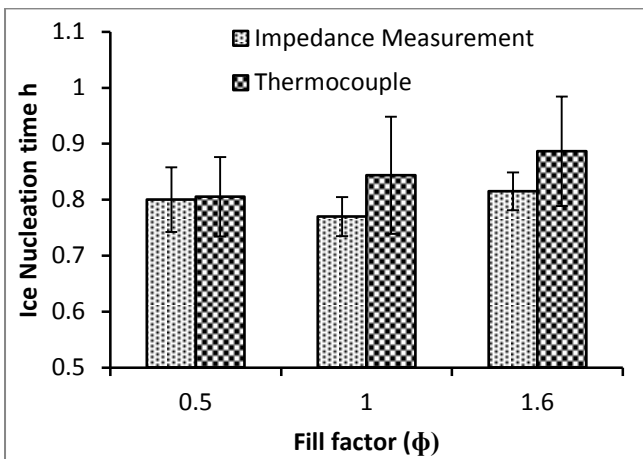


**Figure 4.** Time profiles of (I)  $f_{\text{peak}}$  and (II) temperature for 30mg/ml sucrose during freezing at different fill factors ( $\phi = 0.5, 1$  and  $1.6$ ). ( $n = 10$ ) Note that time zero is taken from the end of the equilibration phase after the vial and contents have been equilibrated at  $25\text{ }^{\circ}\text{C}$  for 10 min.

The results from the perspective of ice nucleation time suggest that there appears to be little influence of fill height on the onset time. This observation is consistent with the fact that freezing starts from the base of the vial, and so the fill height has little bearing on when the initiation of the ice nucleation event occurs. Although one could argue that, the greater the fill volume, the longer it will take to cool the product to the nucleation temperature. However, the overlapping standard deviation values preclude the drawing of any definitive conclusion.

The results from ice nucleation time might also suggest an earlier ice nucleation in the impedance spectroscopy measured vials compared to thermocouple TC, however these observation remain inconclusive due to a high degree of variation in the onset of formation signified by the overlapping standard deviation values.

206 The scatter in the ice nucleation (Fig 5) for any particular fill volume confirms the stochastic nature of the ice  
 207 nucleation process (25) (%COVs range from 12.4 to 8.8 for the thermocouple data and 7.2 to 4.1 for the IS data).  
 208 This inherent variability in the onset of ice formation could result in differences in the degree of super-cooling and  
 209 hence different ice morphologies in the frozen matrix. The fact that the scatter in the onset is greater for the TC data  
 210 than the IS data may be due to the fact that the TC measurement is more sensitive to its position in the vial in  
 211 relation to the spatial seeding of the ice layer.



212  
 213 **Figure 5** Ice nucleation time for sucrose 30mg/ml at different fill factors. Time zero is taken from the end of the  
 214 equilibration phase after the vial and contents have been equilibrated at 25 °C for 10 min. The nucleation time is  
 215 then calculated from the time point B (Fig. 3).

216  
 217 By plotting the freezing time, the solidification time and the equilibration time (from both the fpeak derived-  
 218 estimates and thermocouple derived-estimates) shows that the duration of each phase has a broadly linear  
 219 dependance on fill factor (fig 6). The solidification time almost doubles with a doubling of the fill factor as one might  
 220 expect. However, the equilibration time is much less dependent on the fill factor. The fact that the equilibration time  
 221 is almost constant might mean that this time equates to the time required for the excess heat to pass through the  
 222 base of the vial and to some extent through the walls of the vial. As the volume of the frozen mass increases there is  
 223 a small increase in the contribution from the vial, which is associated with the increased wall volume that is adjacent  
 224 to the liquid fill. The intercept on the y-axis can then be considered as the time constant for heat flux through the  
 225 base and the gradient of the line is the time constant for heat flux through unit area of the side walls of the vial.

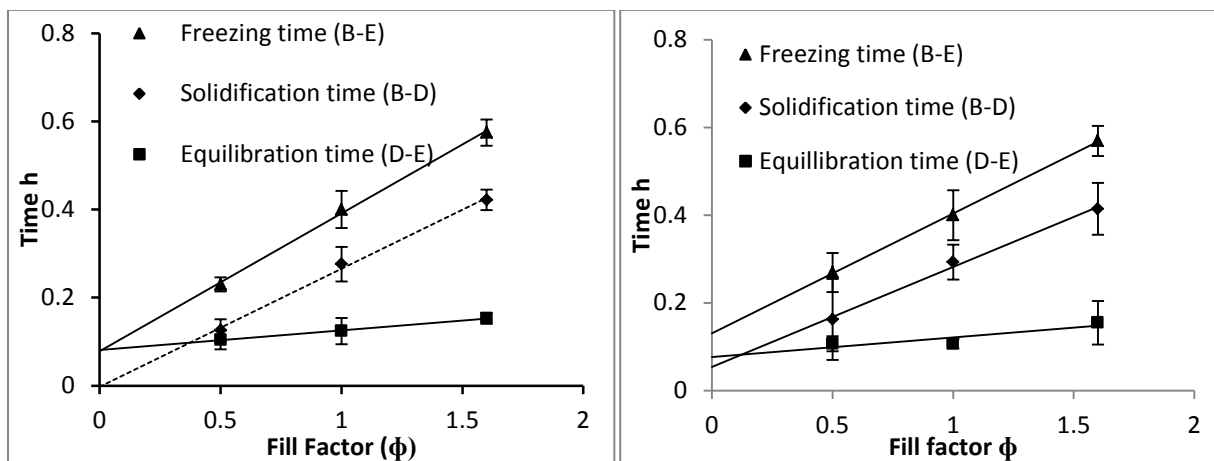


**Figure 6** Freezing time, solidification time and equilibration time for 3% w/w sucrose solution at different fill factors ( $n = 10$ ), (LEFT) Impedance measurement (RIGHT) Thermocouple measurement.

The line of best fit to the IS derived solidification time extrapolates back to zero whereas the line of best fit for the TC derived solidification time does not extrapolate to zero. This observation suggests a potential limitation of the point measurement systems, whereby the position of the thermocouple in relation to the fill volume and the walls of the vial will impact the time point at which any one particular phase is deemed to have completed.

In contrast, the improved linearity between the time duration of the solidification phase and the fill volume, as derived from the log peak values, is a consequence of the fact that the impedance measurement is sensing the entire fill volume (Given that the guard electrode surrounds the measurement electrodes then this will force the field lines through the contents of the vial and hence the impedance measurements sense the entire contents of the vial).

From this work and other recent publications (24) it is becoming clear that the through-vial impedance spectroscopy technique may have a role to play in the development of lyophilization processes and formulations. In particular it may find a useful role in defining the *in situ* characteristics of the freezing process, especially in regard to the manifestation of first and second order transitions such as eutectic crystallation (data not presented) and the glass transition (26) and the impact of various process conditions (set temperatures and ramp rates) including those which define the process of annealing. Further development of the technology to establish a non-contact measurement may even allow for the technique to be used more extensively in the processes of scale up.



245 A major advantage over other single vial measurement techniques (such as NIR, microbalance) is that vials may be  
246 clustered in the usual hexagonal array (which is employed when the shelf is fully loaded) as a consequence of the  
247 minimal physical space taken up by the electrode system. The major disadvantage (as with all single vial  
248 measurements) is that only a limited number of vials may be characterised which makes extrapolation to the whole  
249 batch somewhat difficult. However, further development of the technology to establish a non-contact measurement  
250 may allow for multiple vials to be assessed within domains of the freeze-drier. Such a development would then  
251 render the technique more applicable to scale up and process verification in GMP freeze-driers.

## 252 **Conclusion**

253 Impedance spectra from the electrode-vial-solution assembly displayed a pseudo-relaxation process which arises  
254 from the polarization of the solution-glass wall interface. Of the two parameters characterising the process (i.e. peak  
255 frequency,  $f_{\text{peak}}$ , and peak amplitude,  $C''_{\text{peak}}$ ) it is  $f_{\text{peak}}$  that shows a strong correlation with the solution temperature  
256 as recorded by the thermocouple. The time profile of  $f_{\text{peak}}$  during the freezing process recorded the various phases of  
257 (i) cooling, (ii) ice nucleation and growth leading to the solidification of the product, and (iii) the equilibration of the  
258 frozen solution with the shelf temperature. A linear relationship between the duration of the solidification phase and  
259 fill volume suggests that fixed electrode geometries may be used to investigate a range of fill volumes. The extension  
260 of these studies to lower temperatures (i.e. temperatures below  $T_g$  and  $T_c$  for sucrose and other materials), so that  
261 the technique might be used to track the primary drying stage, are described elsewhere in (24) and (26).

## 262 **Acknowledgements**

263 The current impedance measurement system (LyoDEA™) was developed through collaboration with GEA Pharma  
264 Systems, AstraZeneca, and Ametek, and co-funded by the Technology Strategy Board.

## 265 **References**

- 266 1. Pikal MJ. Freeze Drying. In: Swarbrick J, editor. Encyclopedia of Pharmaceutical Technology, Third Edition.  
267 New York: Marcel Dekker; 2002. p. 1807-33.
- 268 2. James A. Searles JFC, Theodore W. Randolph. The Ice Nucleation Temperature Determines the Primary  
269 Drying Rate of Lyophilization for Samples Frozen on a Temperature-Controlled Shelf. J Pharm Sci. 2001;90(7):860-71.
- 270 3. Hottot A, Vessot S, Andrieu J. Freeze drying of pharmaceuticals in vials: Influence of freezing protocol and  
271 sample configuration on ice morphology and freeze-dried cake texture. Chem Eng Process. 2007;46(7):666-74.

- 272 4. Wilson PW, Heneghan AF, Haymet ADJ. Ice nucleation in nature: supercooling point (SCP) measurements and  
273 the role of heterogeneous nucleation. *Cryobiology*. 2003;46(1):88-98.
- 274 5. Rambhatla S, Ramot R, Bhugra C, Pikal M. Heat and mass transfer scale-up issues during freeze drying: II.  
275 Control and characterization of the degree of supercooling. *AAPS PharmSciTech*. 2004;5(4):54-62.
- 276 6. Liu J, Viverette T, Virgin M, Anderson M, Dalal P. A Study of the Impact of Freezing on the Lyophilization of a  
277 Concentrated Formulation with a High Fill Depth. *Pharm Dev Technol*. 2005;10(2):261-72.
- 278 7. Guttzeit M. Designing An Effective PAT-Driven Scale-Up Of Lyophilization Processes *PharmTechnol*.  
279 2010;22(11):8.
- 280 8. Oetjen G-W. *Foundations and Process Engineering. Freeze-Drying*. Weinheim: Wiley-VCH Verlag GmbH;  
281 2007. p. 1-126.
- 282 9. Mousavi R, Miri T, Cox PW, Fryer PJ. A Novel Technique for Ice Crystal Visualization in Frozen Solids Using X-  
283 Ray Micro-Computed Tomography. *J Food Sci*. 2005;70(7):e437-e42.
- 284 10. Ward KR, Matejtschuk P. The Use of Microscopy, Thermal Analysis, and Impedance Measurements to  
285 Establish Critical Formulation Parameters for Freeze-Drying Cycle Development. In: Rey L, May JC, editors. *Freeze*  
286 *Drying/Lyophilization of Pharmaceutical and Biological Products*. New York: Marcel Dekker; 2010. p. 112-35.
- 287 11. Kasper JC, Friess W. The freezing step in lyophilization: Physico-chemical fundamentals, freezing methods  
288 and consequences on process performance and quality attributes of biopharmaceuticals. *Eur J Pharm Biopharm*.  
289 2011;78(2):248-63.
- 290 12. Konstantinidis AK, Kuu W, Otten L, Nail SL, Sever RR. Controlled nucleation in freeze-drying: Effects on pore  
291 size in the dried product layer, mass transfer resistance, and primary drying rate. *J Pharm Sci*. 2011;100(8):3453-70.
- 292 13. Franks F. *Freeze-drying of Pharmaceuticals and Biopharmaceuticals*. Cambridge: The Royal Society of  
293 Chemistry,; 2007.
- 294 14. Brülls M, Folestad S, Sparén A, Rasmuson A. Near-Infrared Spectroscopy Monitoring of the Lyophilization  
295 Process. *Pharm Res*. 2003;20(3):494-9.
- 296 15. Mujat M, Greco K, Galbally-Kinney KL, Hammer DX, Ferguson RD, Iftimia N, et al. Optical coherence  
297 tomography-based freeze-drying microscopy. *Biomed Opt Express*. 2012;3(1):55-63.
- 298 16. De Beer TRM, Vercruyse P, Burggraeve A, Quinten T, Ouyang J, Zhang X, et al. In-line and real-time process  
299 monitoring of a freeze drying process using Raman and NIR spectroscopy as complementary process analytical  
300 technology (PAT) tools. *J Pharm Sci*. 2009;98(9):3430-46.
- 301 17. Macdonald JR, Johnson WB. *Fundamentals of Impedance Spectroscopy*. In: Evgenij Barsoukov, Macdonald  
302 JR, editors. *Impedance spectroscopy Theory, experiment and applications*. 2 ed. New Jersey: Wiley interscience;  
303 2005. p. 595.
- 304 18. Suherman PM, Smith G. A percolation cluster model of the temperature dependent dielectric properties of  
305 hydrated proteins. *Journal of Physics D-Applied Physics*. 2003;36(4):336-42.
- 306 19. Petrovsky V, Jasinski P, Dogan F. Effective dielectric constant of two phase systems: Application to mixed  
307 conducting systems. *Journal of Applied Physics*. 2012;112(3):034107.
- 308 20. Ermolina I, Smith G. Dielectric spectroscopy of low-losses sugar lyophiles: III: The influence of moisture on  
309 the dielectric response of freeze-dried lactose. *J Non-Cryst Solids*. 2011;357(2):671-76.
- 310 21. Soley A, Lecina M, GÃ¡mez X, CairÃ³ JJ, Riu P, Rosell X, et al. On-line monitoring of yeast cell growth by  
311 impedance spectroscopy. *J Biotechnol*. 2005;118(4):398-405.
- 312 22. Olmi R, Meriakri VV, Ignesti A, Priori S, Riminesi C. Monitoring alcoholic fermentation by microwave  
313 dielectric spectroscopy. *J Microw Power Electromagn Energy*. 2007;41(3):37-49. Epub 2008/03/21.
- 314 23. Smith G, Polygalov E, Page T, inventors; GEA Pharma Systems Limited, assignee. Electrical monitoring of a  
315 lyophilization process Great Britain patent GB2480299. 2011 16/11/2011.
- 316 24. Smith G, Polygalov E, Arshad MS, Page T, Taylor J, Ermolina I. An impedance-based process analytical  
317 technology for monitoring the lyophilisation process. *Int J Pharm*. 2013;449(1-2):72-83.
- 318 25. Nakagawa K, Hottot A, Vessot S, Andrieu J. Modeling of freezing step during freeze-drying of drugs in vials.  
319 *AIChE J*. 2007;53(5):1362-72.
- 320 26. Smith G, Arshad MS, Polygalov E, Ermolina I. An application for impedance spectroscopy in the  
321 characterisation of the glass transition during the lyophilization cycle: The example of a 10% w/v maltodextrin  
322 solution. *Eur J Pharm Biopharm*. 2013.

323

324

325 **Appendix 1:** Estimation of the peak frequencies of liquid and frozen sucrose solution (30 mg/ml)  
326 within tubing vial of different vial geometries

327 In a simple approximation, the impedance of the object under test can be described as a  
328 combination of resistor and capacitor; the resistance of which is defined by following equation

$$329 \quad R = K_1 d / A_{CS} \sigma \quad (1)$$

330 where  $K_1$  is a geometrical coefficient,  $d$  is the internal diameter of the vial,  $A_{CS}$  is an area of effective  
331 vertical cross section of the sample (i.e. the solution within the vial) and  $\sigma$  is specific conductivity of  
332 the sample. The capacitance can be defined by the following equation.

$$333 \quad C = \epsilon_0 \epsilon A / l \quad (2)$$

334 Where  $\epsilon_0$  is the permittivity of a vacuum,  $\epsilon$  is the dielectric constant of glass,  $A$  is the area of the  
335 electrodes and  $l$  is thickness of the glass wall. For the purpose of these calculations, the wall  
336 thickness is assumed to be constant for all sizes of vial.

337 Multiplying  $R$  by  $C$  we obtain

$$338 \quad \tau = RC = K_1 \epsilon_0 \epsilon d A / \sigma l A_{CS} \quad (3)$$

339 where  $\tau$  is the known as the time constant of the serial RC circuit. It is this time constant which  
340 defines the position of the interfacial relaxation peak in the experimental frequency window (where  
341  $f_{peak} = 1/2\pi\tau$ ).

342 In a first approximation  $A_{CS}$  can be presented as  $A_{CS} = AK_2$  where  $K_2$  is a constant coefficient  
343 (associated with the fixed cylindrical shape of the sample volume). Then (3) can be rewritten as

$$344 \quad \tau = RC = K_1 \epsilon_0 \epsilon d A / \sigma l A K_2 \quad (4)$$

345  $A$  in the numerator and denominator can be cancelled thus giving

$$346 \quad \tau = RC = K_1 \epsilon_0 \epsilon d / \sigma l K_2 \quad (5)$$

347 For simplicity let us denote

$$348 \quad K_p = K_1 \epsilon_0 \epsilon / \sigma l K_2 \quad (6)$$

349 Since all members in the right side of (6) are constants then  $K_p$  (the proportionality coefficient) is also  
350 a constant, and expression 5 can be simplified to

$$351 \quad \tau = K_p d \quad (7)$$

352 and respectively

$$353 \quad F_{peak} = 1/2\pi\tau = 1/2\pi K_p d \quad (8)$$

354 Expression 8 shows that the frequency position of the peak has an approximately inverse  
 355 dependence on the internal diameter of the vial.

356 Having measured the experimental value of  $f_{\text{peak}}$  for a 10 ml ( $f_{\text{peak}10\text{ml}}$ ) it is then straight forward to  
 357 estimate  $F_{\text{peak}(x\text{ml})}$  for different sized vials from the ratio of the diameters, according to the formula  
 358 below.

359 
$$f_{\text{peak}x} = f_{\text{peak}(10\text{ml})} \times d_{10\text{ml}} / d_{x\text{ml}} \tag{9}$$

360 Table 1 gives theoretical estimates for the peak frequency for different sized vials, for both the liquid  
 361 state and the frozen state.

362 Table1 estimated position of pseudo-relaxation peak for a 10% solution of sucrose in distilled water  
 363 within glass tubing vials of varying diameter (but constant wall thickness: 2 mm). \* Values of  $f_{\text{peak}}$  for  
 364 a 10% sucrose solution in the 10 ml tubing vial (Schott) have been determined experimentally

Vial size (ml) Schott	internal diameter (mm)	$F_{\text{peak liq}}$ (kHz)	$F_{\text{peak Frozen}}$ (kHz)
10	21.95	64.021	1.390
2	13.91	101.056	2.194
4	13.92	100.959	2.192
6	19.92	70.579	1.532
8	19.90	70.626	1.533

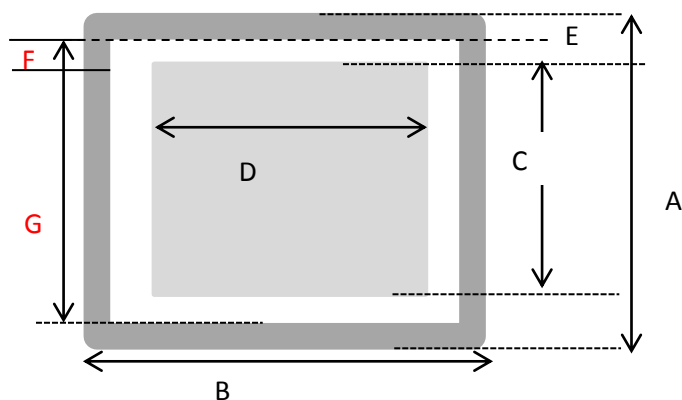
365

366 **Appendix 2:**

367 Thermal Mass Contributions from the External Electrodes

368 The basis for these calculations is to first determine the position of the top of the guard electrode  
 369 from the base of the vial (Fig. 1, dimension A) for a fill volume that provides a constant ratio of the  
 370 liquid cross sectional area to the liquid fill height, for all sizes of vial and which is equal to that for a 3  
 371 ml fill volume in a 10 ml vial.

372



373

374

375 Figure 1 Schematic of the electrode assembly. A: electrode height, B length of guard electrode, C height of  
 376 stimulating/sensing electrode, D width of stimulating/sensing electrode, E width of guard electrode, F spacing  
 377 between guard electrode and sensing electrode, G is the height of the side segment of the guard electrode

378 Once the position of the top of the guard electrode is defined then the next step is to estimate the  
 379 length of the sensing/stimulating electrode (dimension D, Fig. 1). This dimension is defined by the  
 380 ratio of the electrode length to the circumference of the vial, which is fixed at 0.4 for all vials. All  
 381 other dimensions, i.e. the separation/gap between the guard and the sensing/stimulating electrodes  
 382 and the width of the guard electrode are fixed at 1 and 1.5 respectively. Knowing the dimensions A,  
 383 D, E, and F permits the calculation of all other dimensions, from which the total area of the electrode  
 384 assembly can then be calculated (Table 1). The mass of the electrode assembly is then determined  
 385 from the specific weight of the electrode material (0.4 mg/mm<sup>2</sup> for the copper foil used on the 10 ml  
 386 vial) and the % increase in vial weight from attaching the copper foil is then determined from the  
 387 weight of the vial. Table 2 shows the dimensions of the electrode assemblies and the results of these  
 388 calculations of % increase in mass.

389 Table 1 Calculation of liquid cross sectional area (a) and liquid fill height (h) corresponding to a fixed  
 390 ratio of a/h=45 mm

vial size	Mean Wt (g)	± SD (Wt)	Mean diameter (mm)	±SD (Diameter)	a:Mean area of liquid (mm <sup>2</sup> )	± SD (Area)	h:Mean liquid Fill height (mm)	± SD (fill height)
2	4.420	0.014	15.950	0.010	199.833	0.251	4.433	0.006

4	5.584	0.034	15.983	0.042	200.669	1.046	4.451	0.023
6	7.999	0.085	21.937	0.006	377.996	0.199	8.385	0.004
8	8.639	0.084	21.923	0.076	377.537	2.629	8.375	0.058
10	9.283	0.068	23.957	0.061	450.816	2.299	10.000	0.051

391

392

393 Table 2 Theoretical calculations of the % increase in thermal mass on fixing an electrode pair (with  
394 guard electrodes) to different volumes of tubing vial

Vial Size ml	Vial wt (mg)	electro de height mm	sensing electrode			Top and bottom guard electrode			2 side guard electrodes			total area of electrode assembly mm <sup>2</sup>	wt of electrode assembly	thermal mass as % of vial wt
			heig ht (mm )	widt h (m m)	Are a m <sup>2</sup>	heig ht (mm )	widt h (m m)	Are a m <sup>2</sup>	heig ht (mm )	widt h (m m)	Are a m <sup>2</sup>			
2	441 9	4.4	2.22	11	24. 37	1.11	15.9	17. 64	4.7	1.11	5.2 2	94.48	37.793	0.86
4	558 4	4.5	2.23	16.3	36. 34	1.11	15.9	17. 64	4.7	1.11	5.2 2	118.43	47.37	0.85
6	799 8	8.4	4.19	16.3	68. 29	2.09	5	21.7 58	6.5	2.08	13. 52	254.81	101.92	1.27
8	863 9	8.4	4.19	16.3	68. 29	2.09	9	21.7 67	6.5	2.09	13. 59	255.11	102.04	1.18
10	928 2	10	5	18	90	2.5	24	60	7	3	21	342.00	136.8	1.47

395

396 The application of electrodes was practicable by the current method (manually) for vial sizes 6ml,  
397 8ml and 10ml as the dimensions of different electrode components were greater than 1mm  
398 thickness. On contrary for smaller sized glass vials i.e. 2ml and 4ml, dimension electrodes and its  
399 spacing fractionate between 1mm which may require an alternate methodology (sputtering) to  
400 apply thermal mass of the electrode.

401